Research paper

DNA binding and cytotoxicity of some Cu(II)/Zn(II) complexes containing a carbohydrazone Schiff base ligand along with 1,10-phenanthroline as a coligand

Manjuri K. Koley, Natarajan Duraipandy, Manikantan Syamala Kiran, Babu Varghese, Periakaruppan T. Manoharan, Aditya P. Koley

PII: S0020-1693(17)30679-5
DOI: http://dx.doi.org/10.1016/j.ica.2017.06.068
Reference: ICA 17717

To appear in: *Inorganica Chimica Acta*

Received Date: 30 April 2017
Revised Date: 25 May 2017
Accepted Date: 28 June 2017

Please cite this article as: M.K. Koley, N. Duraipandy, M.S. Kiran, B. Varghese, P.T. Manoharan, A.P. Koley, DNA binding and cytotoxicity of some Cu(II)/Zn(II) complexes containing a carbohydrazone Schiff base ligand along with 1,10-phenanthroline as a coligand, *Inorganica Chimica Acta* (2017), doi: http://dx.doi.org/10.1016/j.ica.2017.06.068

DNA binding and cytotoxicity of some Cu(II)/Zn(II) complexes containing a carbohydrazone Schiff base ligand along with 1,10-phenanthroline as a coligand

Manjuri K. Koley[a,*], Natarajan Duraipandy[b], Manikantan Syamala Kiran[b], Babu Varghese[c], Periakaruppan T. Manoharan[d,*] and Aditya P. Koley[e,*]

[a] Department of Chemical Engineering, Birla Institute of Technology and Science-Pilani, K.K. Birla Goa Campus, Goa 403726, India

[b] Biological Materials Laboratory, CSIR-Central Leather Research Institute, Adyar, Chennai 600 020, India

[c] Sophisticated Analytical Instrument Facility, Indian Institute of Technology-Madras, Chennai 600 036, India

[d] Department of Chemistry, Indian Institute of Technology-Madras, Chennai 600 036, India

[e] Department of Chemistry, Birla Institute of Technology and Science-Pilani, K.K. Birla Goa Campus, Goa 403 726, India

---

Abstract

We report the synthesis, characterization and biological activities of the complexes [Cu(o-phen)HL] (**1**), [Cu(o-phen)LCu(OAc)] (**2**), and [Zn(o-phen)LCu(OAc)] (**3**), where, H_3L = *o*-$HOC_6H_4C(H)=N-NH-C(OH)=N-N=C(H)-C_6H_4OH$-*o*, *o*-phen = 1,10-phenanthroline, and OAc = CH_3COO^-. The free ligand and compound **3** have been characterized by X-ray crystallography. A four-line EPR pattern originating from the interaction of the unpaired electron with the central $^{63/65}$Cu nucleus (I = 3/2) with the isotropic coupling constant (A_{iso}) value of 80±1.5 G at RT for compound **1** in DMF suggests its monomeric nature in solution. These compounds undergo irreversible oxidation-reduction. Biological studies show intercalative DNA binding and remarkable cell cytotoxicity as well as anticancer activity. The IC_{50} values of **1**, **2** and **3** for the human lung cancer A549 cell line (0.440, 0.220, and 4.80 μM, respectively) and for the breast cancer MCF7 cell line (2.7, 4.1, and 3.6 μM, respectively) are found to be very promising and appear to be more potent than some anticancer drugs tested for these cell lines. Most importantly, **3** is found to be remarkably less toxic for HaCaT

and L132 normal cell lines as evident from the cell viabilities of these two cell lines in presence of this compound.

Keywords: Cu(II)/Zn(II) complex; EPR and electronic spectra; DNA binding; MTT assay; Cytotoxicity and anticancer activity

---

*Corresponding authors. Email: manjuri@goa.bits-pilani.ac.in (M. K. Koley); ptm@iitm.ac.in (P.T. Manoharan); koleyap@yahoo.co.in (A.P. Koley)

1. Introduction

In recent years there have been increasing efforts to design and develop metal complexes that show DNA binding property, nucleic acid cleavage activity as well as cytotoxicity in order to explore the possibility of finding new metallodrugs that may serve as anticancer agents [1–13]. Many of these works [14–22] are based on bio-essential metal ions, Zn(II) and Cu(II) in particular since these are the second and third most abundant transition metal ions that are present in the cellular body after iron. DNA is an important target for anticancer drugs and the nature of the ligand present in the metallodrugs plays an important role in the binding of the metal complex to DNA (or protein) [23, 24]. Metal complexes with extended planar aromatic ligands bind to DNA in a non-covalent [25–27] manner, either through intercalative or partial intercalative binding, but metal complexes with non-planar ligands are normally found to bind to DNA but not by intercalation. The metal ion also may play an important role in the efficacy of the metal complex as a drug. Cu(II) being a redox active metal ion may promote transformation of DNA or protein through an oxidative pathway whereas Zn(II), being redox inactive is expected to operate in a different pathway [15b]. In our continuing interest and effort in designing and developing metal complexes with suitable donor ligands with additional heterocyclic N-donors [28], that are capable of effectively binding and cleaving DNA, we have synthesized a few Cu(II)/Zn(II) complexes with a carbohydrazone ligand because carbohydrazones (and also thiocarbohydrazones) are known to be a class of fascinating ligand

systems in the field of coordination chemistry with their versatile structural conformations and possess several donor sites [29]. Here, we present the synthesis, spectral (ESI-MS, UV-visible, IR, and EPR), electrochemical and the biological activities of three compounds of Cu(II)/Zn(II) containing the enol form of the Schiff base ligand 1,5-bis(salicylidene)carbohydrazide and 1,10-phenanthroline as a coligand.

2. Results and discussion

We have studied the reactions of $Cu(OAc)_2 \cdot H_2O$ and $Zn(OAc)_2 \cdot 2H_2O$ with 1,5-Bis(salicylidene)-carbohydrazide (A) in methanol to prepare the complexes of the corresponding Schiff base B or B′ as shown in Fig.1 in its enol form in 1:1 or 2:1 (M:L) ratio to prepare the corresponding mononuclear or dinuclear complexes, respectively. The ligand in its enol form can exist either in syn or anti with two distinctly different coordination sites [29]. The site 1 is characterized by one phenolate O^-, one enolate O^- and one imine N, while the site 2 is characterized by one phenolate O^-, one imine N, and another secondary NH donor atom. The different forms of the ligand are shown in Fig. 1.

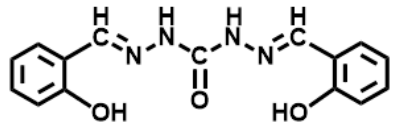

A: keto form

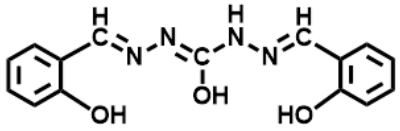

B: enol form (syn)

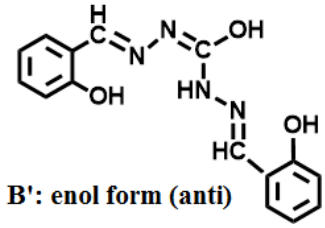

B': enol form (anti)

Fig. 1. Structure of the ligand in its keto and enol forms.

The complexes are poorly soluble in common organic solvents like methanol, ethanol, acetonitrile or dichloromethane but readily soluble in DMSO and DMF. Conductivity measurements with fresh solutions of the compounds **1** - **3** in DMF show these are nonelectrolyte in nature. The ESI-MS spectra (in the positive-ion mode) for complexes **1**–**3** have been recorded in DMSO and the results are presented in Fig. S1 (Supplementary material). Complex **1** showed peaks at m/z 540.33 $[M]^+$, *m/z* 579.19 $[M + K]^+$, compound **2** showed peak at *m/z* 701.77 $[M + K + H]^+$ while complex **3** showed peak at *m/z* 701.70 $[M + K]^+$, respectively. Based on their physico-chemical properties, elemental analyses, mass spectra and X-band RT solution EPR results (vide infra) the proposed structures of **1-3** are shown in Fig. 2.

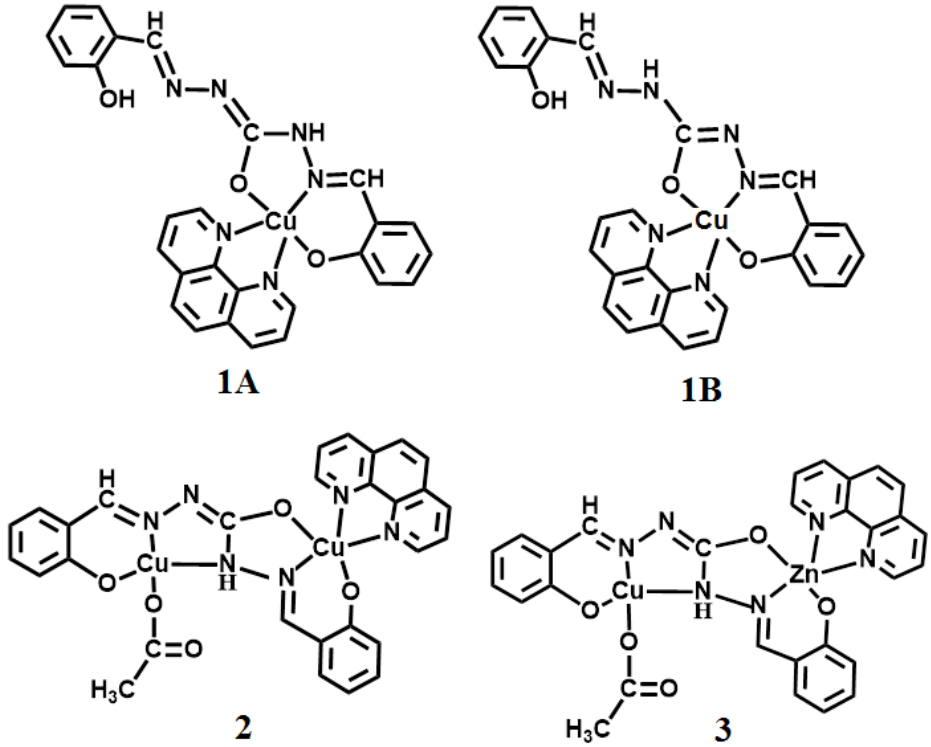

Fig. 2. Proposed structures of the compounds **1-3**.

The IR spectrum of the free ligand (figure not shown) clearly displays the ν(C=O) at 1690 cm^{-1} and ν(C=N) at 1625 cm^{-1}, respectively, clearly suggesting it exists in its keto form [29] and is confirmed from its crystal structure (vide infra). The ν(C=O) band at 1690 cm^{-1} is found to be absent in all three

metal complexes and the ν(C=N) of the free ligand at 1625 cm^{-1} is shifted to 1605 cm^{-1} in the IR spectra of all these complexes indicating the coordination of the imine N to the metal ion. This is confirmed from the crystal structure of **3**. The IR spectra of compounds **2** and **3** in the region 4000-400 cm^{-1} are found to be very similar (Fig. S2, Supplementary material), indicating their structural similarities and similar ligand environments but the IR spectra of **1** and **2** (or **3**), as expected, are different (figure not shown). This difference is originating from the absence of metal ion along with the acetate group in the second site in compound **1**. For example, a sharp peak observed at 3266 cm^{-1} for **1** which is most likely originating from ν(N–H) is found to be absent in the IR spectrum of **2**. Similarly, the peak observed for **2** at 1545 cm^{-1}, possibly associated with the coordinated acetate group is absent in the spectrum of **1**. It is to be mentioned here that there is another possibility for compound **1** having an alternate structure [29] with slight difference in coordination or ligand environment as shown in 1B of Fig. 2. However, it is difficult to differentiate among these two structures (1A or 1B) at this stage in the absence of any crystal structure, though we suggest the possibility of having structure 1A based on the analogy with the crystal structure of **3**. Moreover, the differences in the electronic structures of compounds **1**-**3** are clearly reflected from their electronic spectra shown in Fig. S3 (Supplementary material) as well as from their EPR spectra (vide infra). These compounds exhibit strong LMCT in the visible region, however, the weak ligand field transitions are observed in the 750-550 nm region as evident from Fig. S3 (Supplementary material). Interestingly, these complexes exhibit significant catalytic activity toward the oxidation of catechol in DMSO medium in presence of air. The catecholase activity of the complexes **1** and **2** were studied through the oxidation of model substrate 3,5-di-*tert*-butyl-catechol (3,5-DTBC) under excess substrate conditions. The oxidation product 3,5 -di-*tert*-butylquinone (3,5-DTBQ) has a characteristic absorption band maxima at ~ 401 nm . The electronic spectral change due to the formation of 3,5-DTBQ from the catalytic oxidation of 3,5-DTBC in presence of **1** and **2** were monitored with time and observed spectral changes are shown in Fig. S4 (Supplementary material).

Fig. 3 shows the plot of absorbance change at ~401 nm for the formation of 3,5-DTBQ with time from the catalytic oxidation of 3,5-DTBC in presence of air with **1** in DMSO [0.90×10^{-4} M] (blue circles), **2** in DMSO [0.72×10^{-4} M] (black squares), and also **2** in DMSO:H_3OH (1:9) [0.75×10^{-4} M] (red triangles) and keeping the 3,5-DTBC concentration same [1.10×10^{-2} M] for all three cases. It is evident from Fig. 3 that the catalytic activity of **1** in DMSO toward 3,5-DTBC oxidation in presence of air is slower than that of **2** in DMSO (keeping all other parameters same) based on the rate of absorbance change near 401 nm (Fig. S4, Supplementary material) for the formation of 3,5-DTBQ as reflected in Fig. 3. However, this catalytic oxidation process is found to be much faster and reached the steady state within 10 h when the same reaction was carried out in 9:1 methanol:DMSO medium keeping other parameters same, clearly showing the role of the solvent on their reactivity.

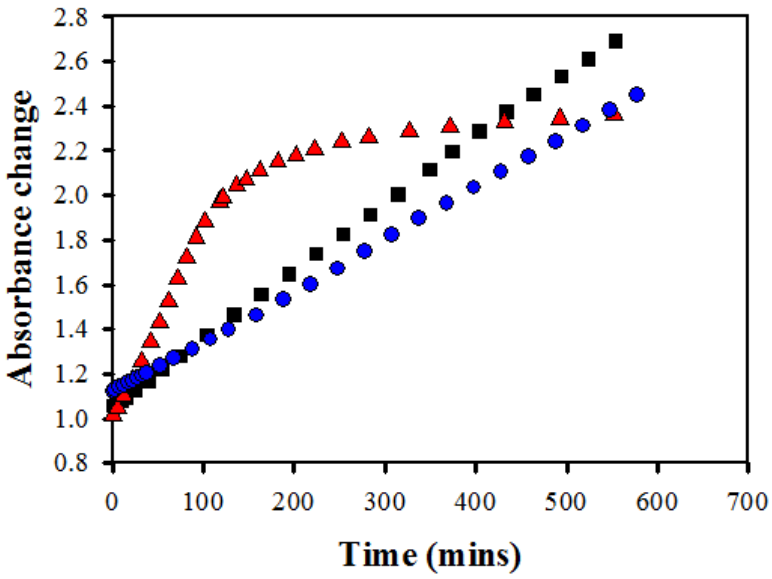

Fig. 3. Plot of absorbance change at ~401 nm for the formation of 3,5-DTBQ from the catalytic oxidation of 3,5-DTBC in presence of air with (1) 0.90×10^{-4} M **1** and 1.10×10^{-2} M 3,5-DTBC in DMSO (blue circles), (2) 0.72×10^{-4} M **2** and 1.10×10^{-2} M 3,5-DTBC in DMSO (black squares), (3) 0.75×10^{-4} M **2** and 1.10×10^{-2} M 3,5-DTBC in CH_3OH : DMSO (9:1) (red triangles).

2.1. Crystal structures of 1,5-Bis(salicylidene)carbohydrazide, (o-$HOC_6H_4CH=NNH)_2C=O$ and [Zn(o-phen)LCu(OAc)]0.5H_2O·0.5CH_3OH

The structure of 1,5-bis(salicylidene)carbohydrazide and compound **3** have been determined by X-ray crystallography. Fig. 4 shows the ORTEP representation of the molecule 1,5-bis(salicylidene)-carbohydrazide with 40% probability ellipsoids [30]. The crystal is indexed in orthorhombic system with space group 'Aba2' and lattice parameters a = 14.5381(18) Å, b = 9.3483(11) Å, c = 10.2927(11) Å, α = 90°, β = 90°, γ = 90°. The bond length and bond angles are given in Table S1 of the Supplementary material. The very symmetrical structure (Fig. 4) of this compound with both same C(8)-N(2) bond distances of 1.365(4) Å clearly suggest its keto form when not coordinated to metal ion. The packing of the molecules in the unit cell is shown in Fig. S5 (Supplementary material).

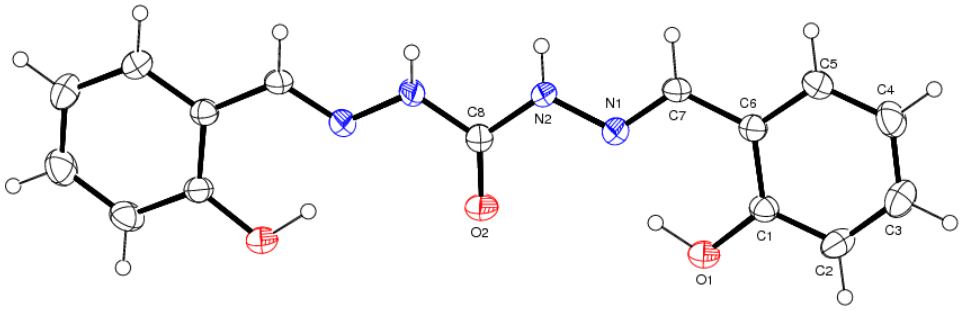

Fig. 4. ORTEP diagram of the compound 1,5-bis(salicylidene)carbohydrazide.

On the other hand, compound **3** crystallizes in triclinic system with the space group Pī. Fig. 5 shows the ORTEP representation of the molecule with 40% probability ellipsoids [30] and packing of the molecules is shown in Fig. S6 (Supplementary material). There are two molecules in the asymmetric unit along with one molecule of methanol and one molecule of water (Fig. 5B). Methanol and water molecules are two-fold disordered (i.e., 50% occupancy each). Cu atoms of both molecules (Cu1 and Cu2) have near square-planar coordination with two nitrogen atoms, one phenolate O^- and one acetate O^- donors (N4N6O3O4 for Cu1 and N10N12O8O9 for Cu2), there is a fifth weak coordination for Cu from the second acetate oxygen (Cu1−O4 = 2.646 (4) Å, Cu2−O10 = 2.668(6)

Å). The mean plane calculation of the basal square plane coordination shows the coordinating N and O atoms to have small tetrahedral distortion (from the ideal square plane). However, the Cu atoms stay in the mean plane (no deviation from the mean plane). Both Zn atoms are five-coordinated. The geometry of coordination is approximately square pyramidal with N1O1N3O2 atoms forming the basal plane for Zn1 and N7O7N9O6 forming the basal plane for Zn2. Both the Zn atoms are slightly shifted in the direction of fifth coordination (from the basal mean plane, domed toward the fifth ligand). All the hydrogens could be located in the difference Fourier map. However, it was decided to fix the hydrogens at geometrically meaningful positions. These atoms were refined by riding model. The packing of molecules in the unit cell shows solvent mediated H-bonding interactions stabilizing the lattice. It is evident from the bond distances of C(20)-N(5) = 1.27(3) Å and C(20)-N(4) = 1.38(3) Å, respectively that the Schiff base ligand is no longer symmetrical after its enolization and coordination to the metal ion(s). Also there are significant differences in bond lengths of C(21)-N(6) = 1.27(3) Å and C(19)-N(3) = 1.36(3) Å, suggesting the differences in the two metal binding sites.

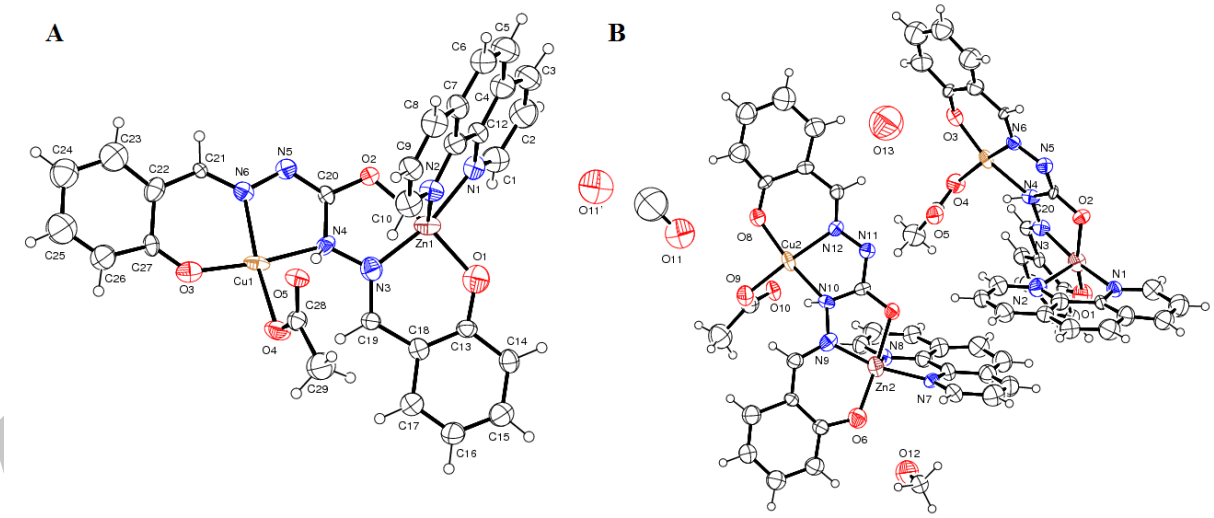

Fig. 5. ORTEP diagram of the compound Zn(o-phen)LCu(OAc)·0.5H_2O·0.5CH_3OH . Selected bond lengths (Å) and angles (^{o}): N(1)-Zn(1), 1.97(3); N(2)-Zn(1), 2.21(3); N(3)-Zn(1), 1.88(3); O(1)-Zn(1), 1.91(2); O(2)-Zn(1), 2.009(18); N(4)-Cu(1), 1.98(2); N(6)-Cu(1), 1.96(2); O(3)-Cu(1),

1.83(2); O(4)-Cu(1), 1.98(2); N(7)-Zn(2), 1.99(2); N(8)-Zn(2), 2.24(2); N(9)-Zn(2), 1.86(2); O(6)-Zn(2), 1.92(2); O(7)-Zn(2), 2.003(19); N(10)-Cu(2), 1.93(2); N(12)-Cu(2), 1.99(2); O(8)-Cu(2), 1.84(2); O(9)-Cu(2), 1.95(2); N(3)-Zn(1)-O(1), 95.6(11); N(3)-Zn(1)-N(1), 166.7(11); O(1)-Zn(1)-N(1), 97.5(10); N(3)-Zn(1)-O(2), 79.9(10); O(1)-Zn(1)-O(2), 161.8(8); N(1)-Zn(1)-O(2), 87.0(9); N(3)-Zn(1)-N(2), 97.5(10); O(1)-Zn(1)-N(2), 112.4(9); N(1)-Zn(1)-N(2), 79.4(10); O(2)-Zn(1)-N(2), 85.7(8); N(9)-Zn(2)-O(6), 96.3(11); N(9)-Zn(2)-N(7), 166.4(11); O(6)-Zn(2)-N(7), 96.5(9); N(9)-Zn(2)-O(7), 78.0(10); O(6)-Zn(2)-O(7), 162.5(9); N(7)-Zn(2)-O(7), 88.4(9); N(9)-Zn(2)-N(8), 99.6(10); O(6)-Zn(2)-N(8), 110.6(9); N(7)-Zn(2)-N(8), 80.0(10); O(7)-Zn(2)-N(8), 86.8(8); O(3)-Cu(1)-N(6), 90.0(10); O(3)-Cu(1)-N(4), 167.6(9); N(6)-Cu(1)-N(4), 81.4(10); O(3)-Cu(1)-O(4), 94.2(9); N(6)-Cu(1)-O(4), 169.9(9); N(4)-Cu(1)-O(4), 95.7(9); O(8)-Cu(2)-N(10), 166.8(9); O(8)-Cu(2)-O(9), 93.3(9); N(10)-Cu(2)-O(9), 95.8(9); O(8)-Cu(2)-N(12), 90.4(10); N(10)-Cu(2)-N(12), 82.1(10); O(9)-Cu(2)-N(12), 170.8(9).

2.2. EPR results

The powder EPR spectra for the compounds **1**-**3** were recorded at room temperature (RT) as well as at liquid nitrogen temperature (LNT) at X-band frequency and are shown in Fig. 6. **1** at RT has a broad line at a g-value of 2.08 (an averaged out g–value) and also a weak forbidden line around 155 mT indicating that it is possibly a dimer. But its EPR at LNT, i.e. **1** at LNT not only shows the forbidden $\Delta Ms = \pm 2$ line at around the same field but also its main g-region is resolved though not clearly. One can possibly account for a seven line not-so-well resolved EPR spectrum in the parallel component, but $g_{\perp}$ does not show any hyperfine line because of line broadening and low value expected for the hyperfine coupling constants in this direction. The EPR spectra of **2** at RT and at LNT almost appear to be the same as the corresponding **1** spectrum. The presence of forbidden $\Delta Ms = \pm 2$ line around g~4 and a reduced hyperfine coupling constant value for $Cu^{63,65}$ make both of them resulting from a dimer of a Cu-Cu interaction. While this is true for the molecule of **2**, it is not

possible for **1** to have such an interaction since there is no such intra-molecular dimer moiety as part of its structural characterization which has only one copper. However, if the molecular packing involves a dimer from two different molecules, then it can also give such an exchange interaction.

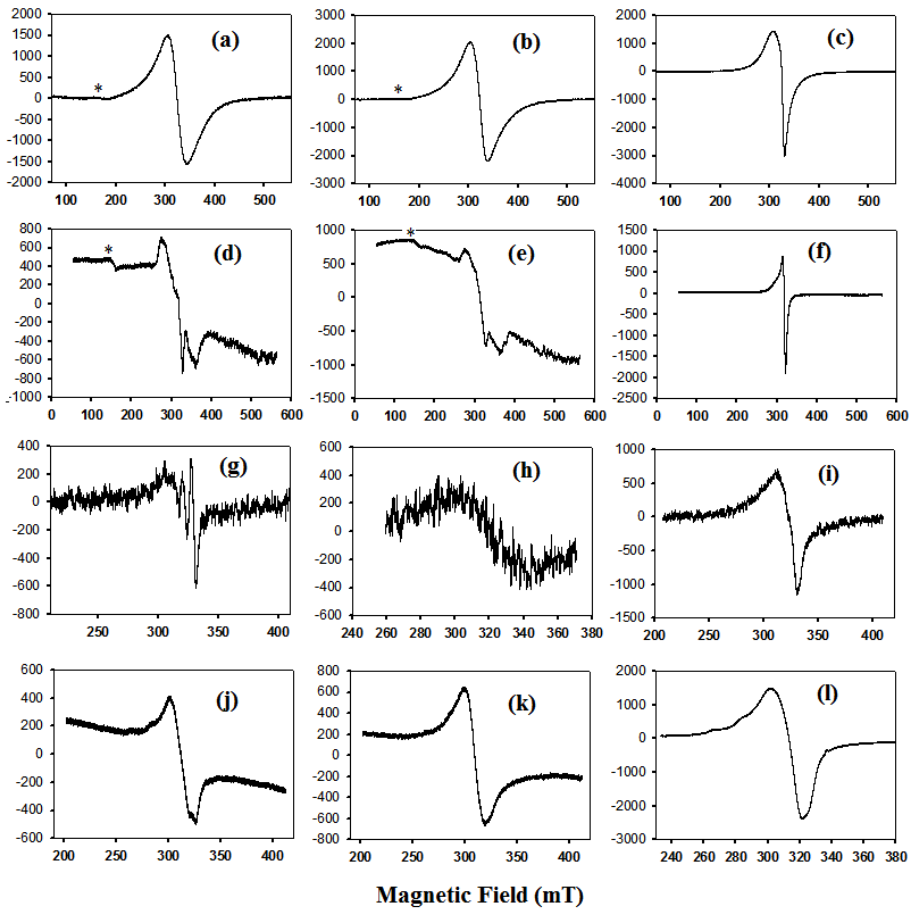

Fig. 6. X-band EPR spectra of the compounds. (a)-(c) are RT spectra for **1**-**3** powder samples, (d)-(f) are LNT spectra for **1**-**3** powder samples, (g)-(i) are RT solution spectra for **1**-**3** in DMF, and (j)-(l) are LNT frozen glass spectra for **1**-**3** in DMF, respectively. * indicates the existence of the forbidden $\Delta Ms = \pm 2$ line around g~4.

On the other hand, **3** at both the RT and LNT do not show either any forbidden line or hyperfine lines. It is understandable from the structure of **3** that the interacting centres involve Cu-Zn instead of Cu-Cu in **2**. Possibly due to line broadening effects due to dipolar interactions in solid state **3** has

just given a broad line both in parallel and perpendicular directions. RT solution EPR shows compound **1** is a monomer of Cu^{2+} and the not so well resolved isotropic hyperfine lines from copper nuclei with A_{iso} being approximately 8 mT with g value around 2.06, typical of a monomeric Cu^{2+} squareplanar or at the most C_{2V} symmetry. The same compound in DMF at LNT gives $A_{\parallel}$ value of ~20 mT with $g_{\parallel} = 2.17$ and $g_{\perp} = 2.04$, respectively. But the same at RT and LNT give similar line but broadened to a whopping width of ~36mT due to dipolar interaction. Compound **2** in DMF, likely to be a dimer, exhibited spectra both at RT and LNT which are clearly one line spectrum with a width of about 35 mT at RT and about 10 mT at LNT. Higher intensity at LNT coupled with sharpening of the line clearly indicates the possibility of its being a weak ferromagnet due to intramolecular exchange coupling. But in solid state, as already mentioned, at RT it gives a strong line with a width of ~35 mT and the existence of the forbidden $\Delta Ms = \pm 2$ line around g~4 resulting from the same intramolecular dimer with exchange coupling due to Cu-Cu interaction. Compound **3** in DMF gives a weak EPR line with unresolved hyperfine at RT but at LNT it becomes a strong line with resolved hyperfine values specially in the parallel section. Possibly it indicates that most of the spin is located in Cu^{2+} probably not leaking to Zn^{2+}. But the powder at RT gives a strong one anisotropic line with no hyperfine lines. The EPR parameters are presented in the following Table 1.

Table 1. EPR parameters derived from the spectra at RT and LNT.

Compound	**$g_{\parallel}$**	**$g_{\perp}$**	**g / g_{av}**	**$A_{\parallel}$**	**$\Delta Ms = \pm 2$**
1-RT	-	-	2.082	-	
1-LNT	2.17	2.040	2.083(g_{av})	11.5 mT	Yes
2-RT	-	-	2.092		
2-LNT	2.19	2.10	2.12 (g_{av})	13.5 mT	Yes
3-RT	2.19	2.07	2.11 (g_{av})		
3-LNT	2.17	2.06	2.097 (g_{av})		

2.3. DNA binding studies

DNA binding studies were performed using UV-Vis spectroscopy. In order to get the binding constants for the compounds **1**-**3**, electronic absorption titration experiments were performed with incremental amounts of calf thymus DNA *(*ct-DNA) in 10 mM Tris–HCl buffer (pH 7.45) and by keeping the individual complex concentration constant. The binding of complexes to the ct-DNA exhibits hypochromism (Fig. 7) with a minor red shift of the band at around 394 nm for **1**, 395 nm for **2**, and 380 nm for **3**, respectively, indicating intercalative binding, resulting in strong stacking between the DNA base and aromatic chromophore [31]. The binding constant K_b has been calculated from the kinetic data obtained using the following equation (1).

$$\frac{[DNA]}{(\varepsilon_a - \varepsilon_f)} = \frac{[DNA]}{(\varepsilon_b - \varepsilon_f)} + \frac{1}{K_b(\varepsilon_b - \varepsilon_f)} \qquad (1)$$

where, [DNA] is the concentration of ct-DNA used, and ε_a, ε_f and ε_b correspond to apparent extinction coefficients for the complex i.e., Abs/[complex] in the presence of DNA, in the absence of DNA and to fully bound DNA, respectively. A plot of [DNA]/($\varepsilon_a - \varepsilon_f$) versus [DNA] yields a slope = 1/($\varepsilon_b - \varepsilon_f$), and the intercept = 1/K_b($\varepsilon_b - \varepsilon_f$), respectively. The binding constant K_b is calculated from the ratio of the slope to the intercept. The binding constant K_b is found to be 1.18×10^5 M^{-1} for **1**, 2.63×10^5 M^{-1} for **2**, and 2.53×10^5 M^{-1} for **3**, respectively. The K_b values are comparable to that reported for a classical intercalator such as ethidium bromide (K_b = 1.40×10^5 M^{-1}) in 25 mM Tris-HCl buffer (pH 7.33) [32]. The higher K_b values for **2** and **3** as compared to **1** suggest that **2** and **3** possessing two metal centres interact with DNA more strongly than complex **1**. Also the K_b values for **2** and **3** are found to be higher than those we reported [28] recently for the mononuclear compounds [Cu(pabt)(Imz)](ClO_4) and [Cu(pabt)(*N*-MeImz)](ClO_4), (Hpabt = *N*-(2-mercaptophenyl)-2'-pyridylmethylenimine, Imz = imidazole, N-MeImz = N-

methylimidazole) both of which were distorted square planar containing a tridentate NNS^- Schiff base ligand and imidazole or N-methylimidazole as the coligand in the fourth position.

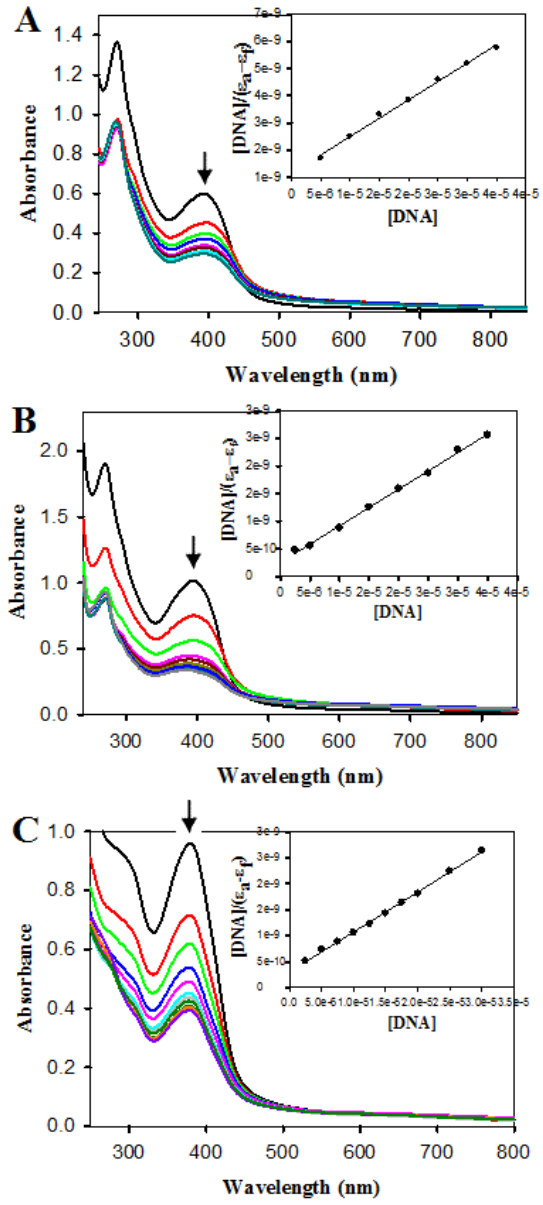

Fig. 7. Change in electronic absorption spectra of **1**-**3** [5×10^{-5} M] upon titration with ct-DNA (0–40 μM) dissolved in 10 mM Tris–HCl buffer (pH 7.45). The arrow shows the decrease in absorbance with respect to an increase in the concentration of ct-DNA. The figure in inset shows the linear fit of $[DNA]/(\varepsilon_a - \varepsilon_f)$ versus [DNA]. The binding constant (K_b) was calculated using the eqn. 1.

2.4. Results on biological activity

2.4.1. Cytotoxicity

The cytotoxicity profiling of the three compounds were evaluated by MTT assay using A549 lung cancer cell line, MCF7 breast cancer cell line, L132 human lung embryonic normal cell line and human keratinocyte HaCaT normal cell line. The cell viability was determined by the reduction of yellow MTT into purple formazan product by the enzymatic activity of mitochondrial dehydrogenase in the live cells. Dose dependent cell death was induced by all three compounds as evidenced from Fig. 8. It was observed that for L132 cell line, compound **2** showed high toxicity at concentration as low as 2.5 μM having cell viability of ~24% while compound **1** showed moderate effect at 2.5 μM when compared to compound **2**. Compound **3** showed much less toxicity even at concentration as high as 10 μM concentration with cell viability of ~55% for the same cell line. Similar result is also obtained with HaCaT cell line in which ~65% cell viability is observed at 10 μM concentration of **3**, whereas **1** and **2** were found to be very toxic even at 2.5 μM concentration. In MCF7 cell line, all three compounds were found to be less toxic at 2.5 μM concentration with cell viability when compared to L132 cell line indicating that these compounds did not have any specificity against breast cancer cell. A549 cell line, compounds **1** and **2** are found to be toxic even at 0.5 μM concentration with cell viabilities of 46% and 39.5%, respectively, while at 2.5 μM concentration the cell viabilities are 30.9% for **1** and 34.25% for **2**, and 62.3% for **3**, respectively. At 5 μM concentration the cell viabilities are 26.6% for **1** and 25.6% for **2**, and 49.1% for **3**, respectively. At 10 μM concentration the cell viabilities are 22.6% for 1 and 24.5% for 2, and 36.7% for **3**, respectively. The cell viability for **3** at 10 μM concentration was found to be as much as 65% (Fig. 8) in HaCaT cell line. Thus, though compounds **1** and **2** are found to be quite toxic for all these cell lines, **3** is found to be less toxic for L132 and HaCaT but possesses good potency for MCF7 and A549 cell lines.

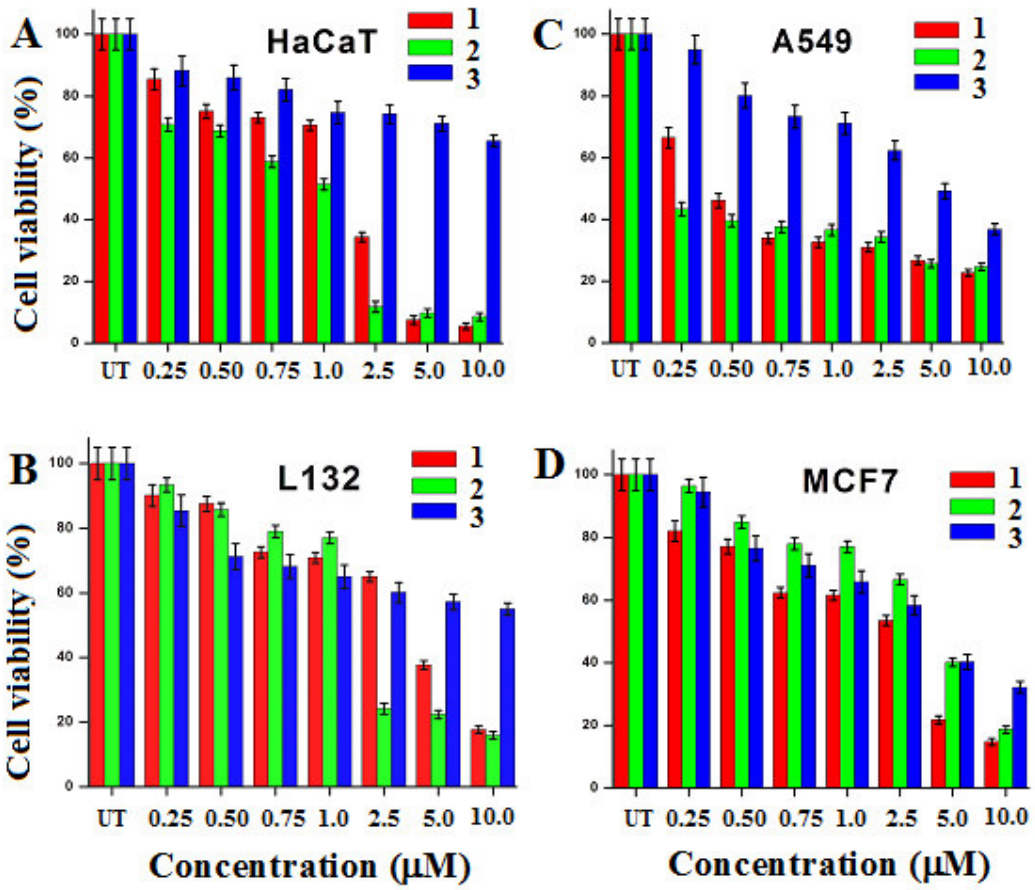

Fig. 8. MTT assay for the compounds **1**-**3**. Panel A. HaCaT cell line, panel B. L132 cell line, panel C. A549 cell line, and panel D. MCF7 cell line.

Fig. 9 shows the plot of cell viability versus concentrations of the compounds **1**, **2**, and **3** for all these cell lines. The IC_{50} values for **1**-**3** calculated from this plot for both the cancer cell lines A549 and MCF7 are presented in Table 2. It is to be noted here that the IC_{50} values for A549 cells are comparable to those reported by Lu et al. [2c] and better than the IC_{50} value reported for cisplatin (4.13 μM for A549). On the other hand, the IC_{50} values for **1**-**3** for MCF7 cell line are found to be higher than that (0.46 μM) reported by Lu et al. [2c] but comparable with that reported for cisplatin (3.92 μM for MCF7) and much lower than that reported for carboplatin (36.65 μM for MCF7) [2c].

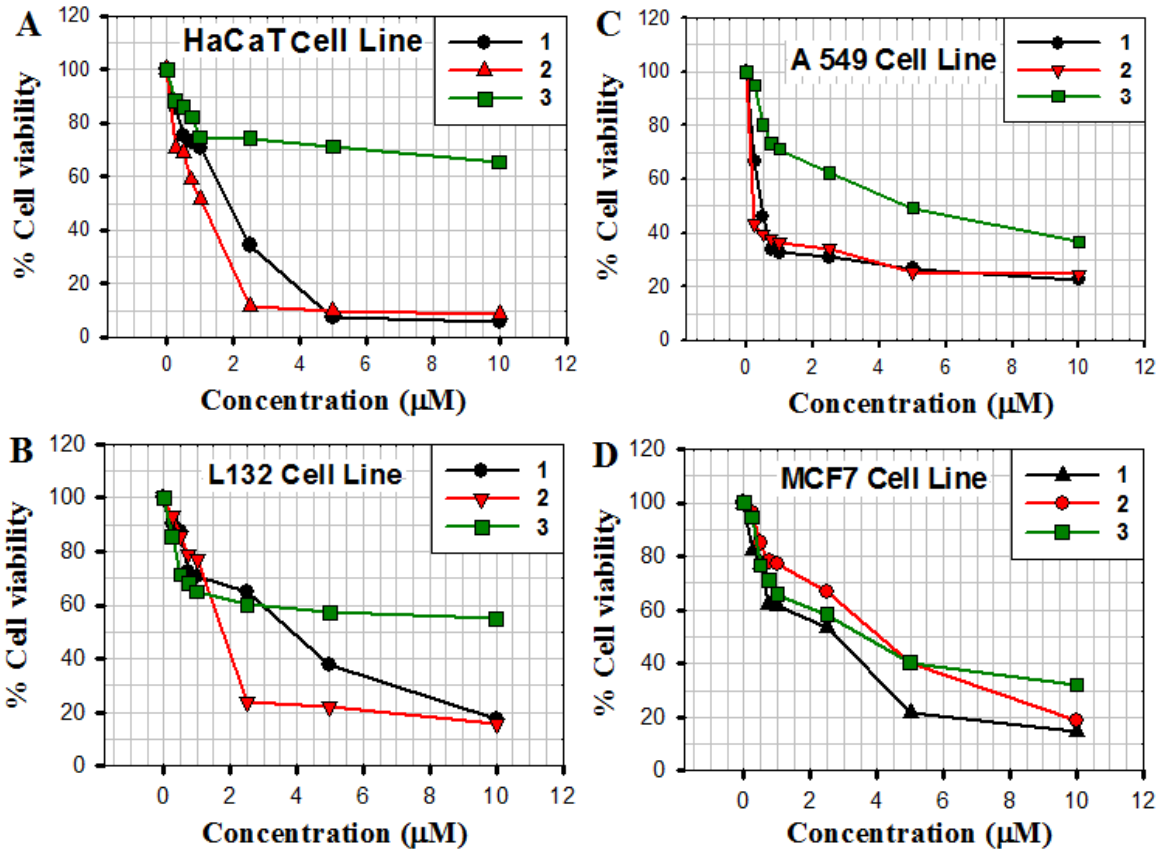

Fig. 9. Plot of cell viability versus concentrations of the compounds **1**, **2**, and **3**: panel A. HaCaT cell line, panel B. L132 cell line, panel C. A549 cell line, and panel D. MCF7 cell line.

Table 2. IC_{50} values for the compounds **1**-**3** calculated from the plot of cell viability versus concentration in the MTT assay.

Compound	IC_{50} in A549 cell line	IC_{50} in MCF7 cell line
1	0.44 µM	2.7 µM
2	0.22 µM	4.1 µM
3	4.80 µM	3.6 µM

2.4.2. Dual-Fluorescence Viability: AO/PI Dual Staining assay for A549 and HaCaT cells

This dual staining assay using the fluorescence microscopy is used to analyze the induction of cell apoptosis in presence of the compounds **1**-**3**. Acridine orange (AO) and propidium iodide (PI) are nucleic acid binding dyes, AO is permeable to both live and dead cells, staining all nucleated cells to

generate green fluorescence but PI enters only in dead, dying, and necrotic nucleated cells with compromised membranes and stains them all generating red fluorescence. But cells stained with both AO and PI together, all dead nucleated cells fluoresce red and all live nucleated cells fluoresce green due to Förster resonance energy transfer (FRET). In this staining method, the following morphological changes were observed (Figs. 10 – 12) in the treated cells: (a) the viable cells with highly organized nuclei fluoresce green as seen from all the control in Figs. 10 – 12; (b) early apoptotic cells with nuclear condensation, that emit orange-green fluorescence; (c) late apoptotic cells with highly condensed or fragmented chromatin and fluoresce orange to red, observed in the treatment with 1 μM concentration of the respective compounds; and (d) necrotic cells fluoresce red with no indication of chromatin fragmentation as clearly evident (Figs. 10 – 11) in the cases of A549 cells treated with 2 μM of each of **1** and **2**, while such red fluorescence is not observed (Fig. 12) with 2 μM concentration for **3** suggesting no or very little DNA damage at this concentration. This is consistent with the cell viability observed from its MTT assay (Fig. 8 panels A, C). All these morphological changes indicate that these complexes might have induced cell death via both apoptosis and necrosis [10b] though the majority of the cells appear to be rounded and shrunken due to apoptosis [1].

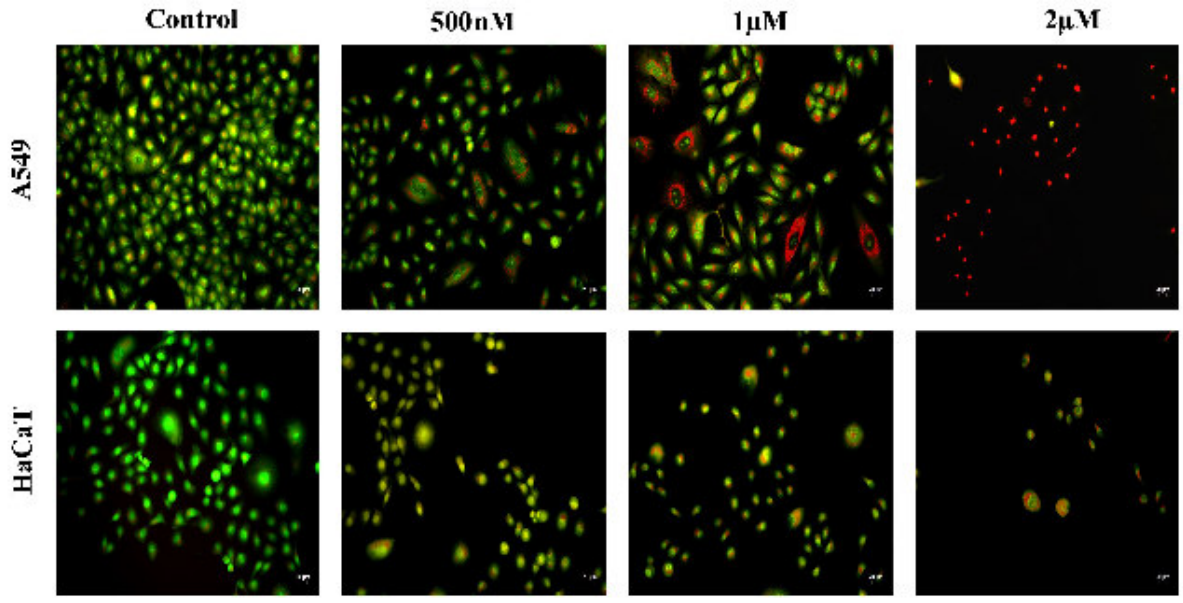

Fig. 10. AO/PI staining results for compound **1** with A549 and HaCaT cell lines. Scale bar: 20 μm.

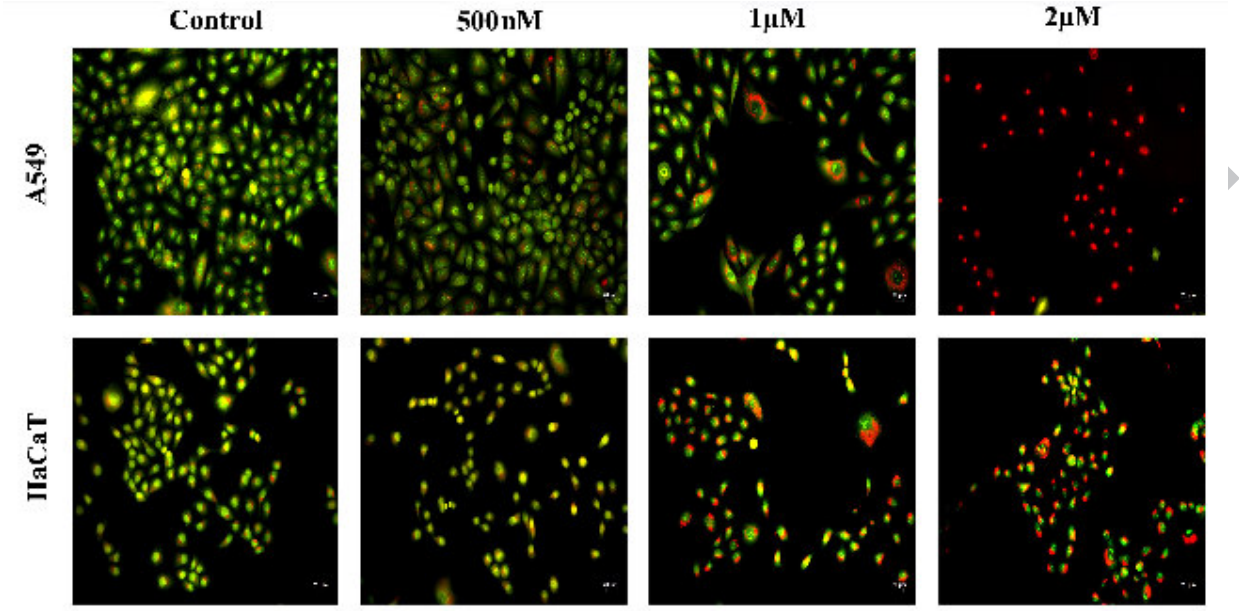

Fig. 11. AO/PI staining results for compound **2** with A549 and HaCaT cell lines. Scale bar: 20 μm.

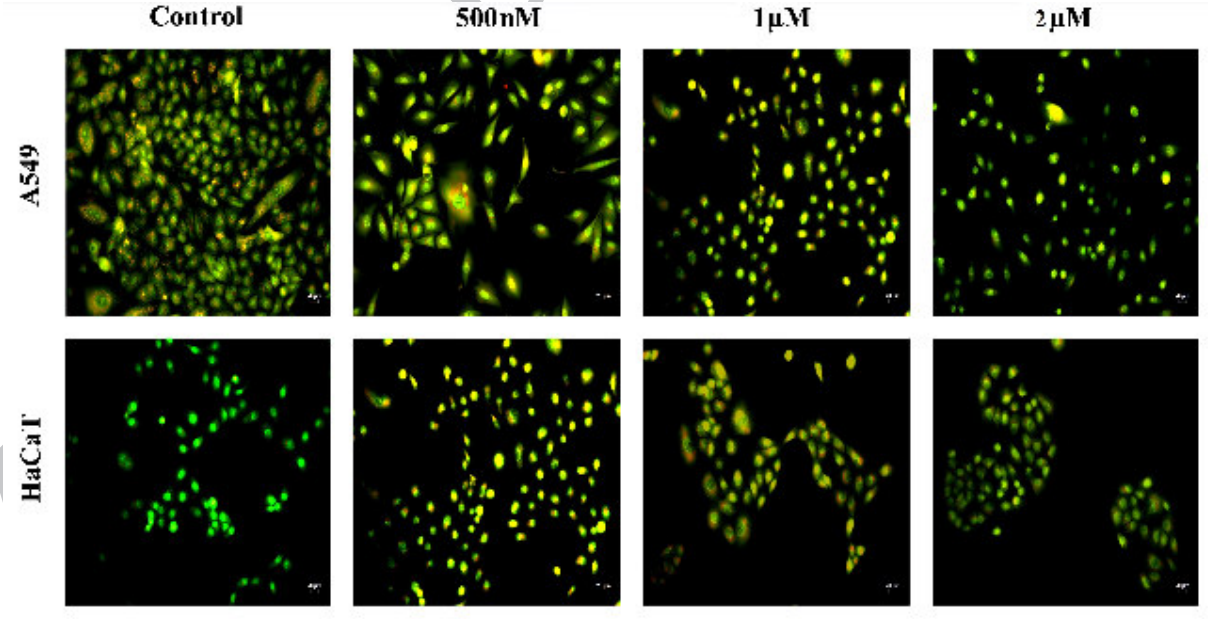

Fig. 12. AO/PI staining results for compound **3** with A549 and HaCaT cell lines. Scale bar: 20 μm.

It is to be noted here that recently Nagababu et al. [1c] have reported the anticancer activity of four mononuclear Cu(II) complexes with some polypyridyl ligands, two of which were found to be highly potent for the anticancer activity. However, these two compounds showed cytotoxicity toward cancerous cell as well as noncancerous cell; and these were comparable to the results obtained with doxorubicin, a FDA approved anticancer drug, which also showed cytotoxicity toward both cancerous and noncancerous cells equally strongly. Based on this, these authors have argued that the possibility of using the compounds synthesized by them as a therapeutic agent cannot be completely ruled out. We also have a very similar situation in our present study, though compound **3**, being much less toxic toward normal cells might be more suitable, but all three compounds can be potential candidates to be tested as therapeutic agents.

2.5. Electrochemical results

The electrochemical behaviour of compounds **1, 2** and **3** have been studied in DMF containing 0.1 M $[N(n\text{-}Bu)_4]ClO_4$ at a platinum working electrode using cyclic voltammetry (CV) in dinitrogen atmosphere. For an initial negative scan compounds **1** and **3** do not show (Fig. 13) any specific reduction wave within 0 to −1.5 V, while compound **2** shows only a broad reduction wave near −1.21 V (versus Ag/AgCl), but no corresponding oxidation peak is observed up to 0.0 V on scan reversal. Compound **1** undergoes two successive oxidations at +0.86 and +1.2 V, while **2** undergoes oxidations at +0.16, +0.89 and +1.30 v, respectively. Compound **3**, on the other hand shows the oxidation waves at +0.55 and +1.28 V, respectively. Reversal of these scans between +1.5 and 0.0 V yielded reduction waves at +0.159 V for **1**, +0.16 V for **2**, and +0.35 V for **3**, respectively (Fig. 13). Scanning between −0.5 and +0.5 V did not show any redox couple in any of these cases (figure not shown). Hence, all these three compounds undergo only irreversible oxidations and reductions.

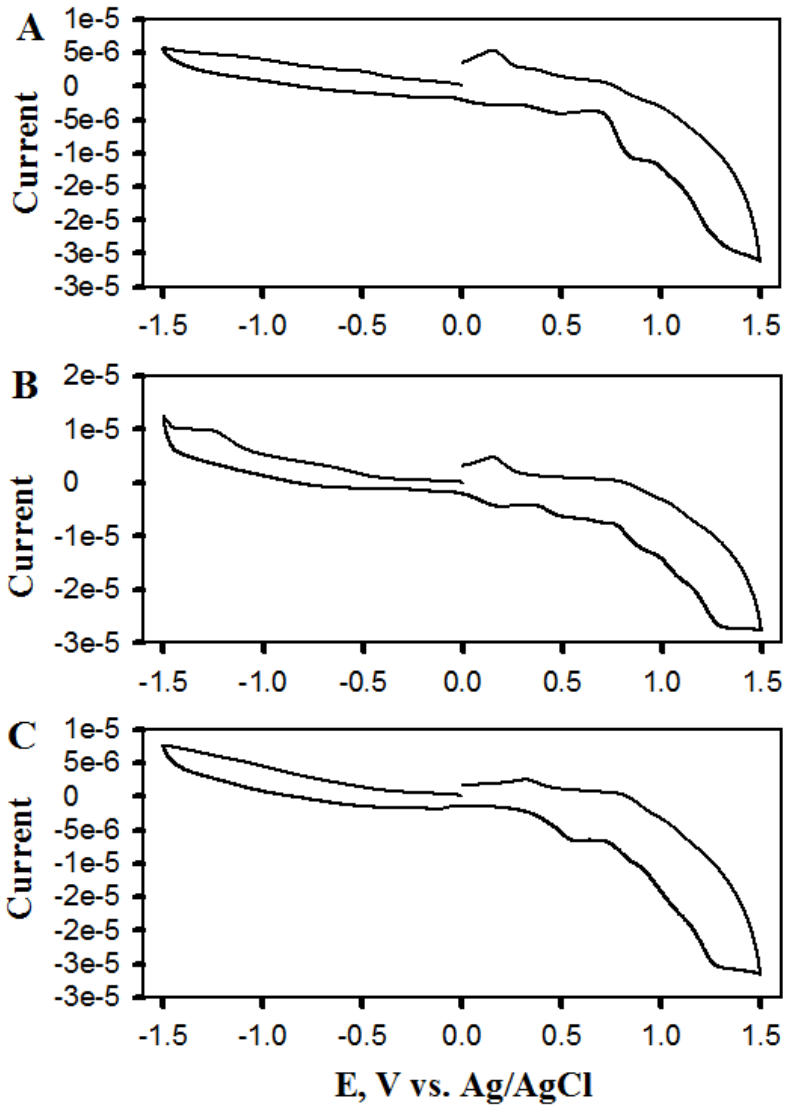

Fig. 13. Cyclic voltammogram of the compounds (1.5×10^{-3} mol L^{-1}) in DMF containing 0.1 M $[N(n\text{-}Bu)_4]ClO_4$ at a scan rate of 100 mV s^{-1}. Panel A for **1**, panel B for **2**, and panel C for **3**.

3. Conclusions

All the three compounds found to have efficient DNA binding capabilities with binding constants ranging from 1.18×10^5 M^{-1} to 2.63×10^5 M^{-1} and they bind to DNA by intercalation mode as revealed from their DNA binding study with calf thymus DNA. The compounds **1**, **2** and **3** exhibited in vitro cytotoxicity against human breast cancer MCF7 cell line and human lung cancer A549 cell

line; as evident from significant decrease in cell viability for doses 0.5-10 μM for both the cell lines; and they are found to be highly potent for both these cell lines as revealed from their IC_{50} values. AO/PI dual staining results strongly suggest the induction of apoptotic pathway for the anticancer activity of these complexes.

4. Experimental

4.1. Chemicals

Carbohydrazide and salicylaldehyde were obtained from Aldrich. Calf thymus DNA was obtained from Sigma, N,N-dimethylformamide (DMF, GR), absolute ethanol, methanol (GR), DMSO, 1,10-phenanthroline monohydrate, $Zn(OAc)_2{\cdot}2H_2O$ and $Cu(OAc)_2{\cdot}H_2O$ (GR) were obtained from Merck.

4.2. Preparation of 1,5-Bis(salicylidene)carbohydrazide, $(o\text{-}HOC_6H_4CH{=}NNH)_2C{=}O$ (H_3L)

This was prepared by modifying the reported method of Bustos et al. [29]. Salicylaldehyde (20 mmol) was added to a solution of carbohydrazide (10 mmol) dissolved in 50 mL of methanol, and the resulting reaction mixture was stirred at RT for 2 h, filtered through a G-3 crucible and the pale white solid was washed well with methanol and air dried. Yield 80%; mp 226 ^{o}C. *Anal*. Calc. for $C_{15}H_{14}N_4O_3$: C, 60.40; H, 4.73; N, 18.78. Found: C, 61.01; H, 4.68; N, 18.51%. Recrystallization of this compound from methanol-ethanol (1:1) mixture led to formation of colorless single crystals suitable for X-ray diffraction. We have characterized it by X-ray crystal structure (vide infra).

4.2. Preparation of the complexes

*4.2.1. [Cu(o-phen)(HL)] (**1**)*

1,10-phenanthroline monohydrate (0.2 g, 0.001 mol) in methanol (10 mL) was very slowly added to a solution of $Cu(OAc)_2{\cdot}H_2O$ (0.2 g, 0.001 mol) in methanol (15 mL) during 20 min with stirring below room temperature (~15 °C) and the dark blue solution was stirred for another 40 min at RT. This blue solution was then added very slowly to a solution of 1,5-bis(salicylidene)carbohydrazide (0.358 g, 0.0012 mol) in 75 mL of methanol during 30 min while the reaction mixture turned bright green. This was stirred for 24 h at RT and the green compound separated from the solution was

filtered through a G-3 sintered glass crucible, washed very well with methanol, air dried, then washed thoroughly with water, and finally washed again with methanol and dried in vacuo. Yield ~65%. *Anal*. Calc. for $C_{27}H_{20}N_6O_3Cu$: C, 60.05; H, 3.73; N, 15.56. Found: C, 59.98; H, 3.75; N, 15.61%. ESI–MS in DMSO: *m/z* 540.33$[M]^+$, *m/z* 579.19 $[M + K]^+$.

*4.2.2. [Cu(o-phen)LCu(OAc)] (**2**)*

1,10-phenanthroline monohydrate (0.2 g, 0.001 mol) in methanol (10 mL) was very slowly added to a solution of $Cu(OAc)_2{\cdot}H_2O$ (0.2 g, 0.001 mol) in methanol (15 mL) during 20 min with stirring below room temperature (~15 °C) and the dark blue solution was stirred for another 40 min at RT. This blue solution was then added very slowly to a solution of 1,5-bis(salicylidene)-carbohydrazide (0.298 g, 0.001 mol) in 50 mL of methanol during 30 min while the reaction mixture turned bright green. This was stirred for 3 h, then $Cu(OAc)_2{\cdot}H_2O$ (0.2 g, 0.001 mol) in methanol (15 mL) was slowly added to this reaction mixture when the solution turned from bright green to dark green. Stirring was continued at RT for 24 h and the dark green compound was filtered, washed well with methanol followed by water and dried in vacuo. Yield: 85%. *Anal.* Calc. for $C_{29}H_{22}N_6O_5Cu_2$: C, 52.65; H, 3.35; N, 12.70. Found: C, 52.51; H, 3.37; N, 13.01%. ESI-MS in DMSO: *m/z* 701.77 $[M + K + H]^+$.

*4.2.3. [Zn(o-phen)LCu(OAc)] (**3**)*

1,10-phenanthroline monohydrate (0.2 g, 0.001 mol) in methanol (10 mL) was very slowly added to a solution of $Zn(OAc)_2{\cdot}2H_2O$ (0.219 g, 0.001 mol) in methanol (15 mL) during 30 min with stirring below room temperature (~15 °C) and the solution was stirred for another 40 min at RT. This colorless solution was then added very slowly to a solution of 1,5-bis(salicylidene)-carbohydrazide (0.298 g, 0.001 mol) in 50 mL of methanol during 30 min while the reaction mixture turned yellow. This was stirred for 6 h, then $Cu(OAc)_2{\cdot}H_2O$ (0.2 g, 0.001 mol) in methanol (15 mL) was slowly added to this reaction mixture when the solution turned dark green. Stirring was continued at RT for 24 h and the dark green compound was filtered through a G-3 sintered glass crucible, and the green

mother filtrate was collected in a 50 mL beaker. The green solid in the crucible was washed very well with methanol, air dried. Then this was washed thoroughly with water, and finally washed again with methanol and dried in vacuo. *Anal.* Calc. for $C_{29}H_{22}N_6O_5ZnCu$: C, 52.50; H, 3.34; N, 12.67. Found: C, 52.41; H, 3.34; N, 12.70%. ESI–MS in DMSO: *m/z* 701.70 $[M + K]^+$.

The green mother filtrate collected in a 50 mL beaker was covered with a watch glass and left for slow evaporation at RT when very thin dark blue crystals were obtained within 3-4 days and were used for X-ray crystallography. This is to be noted here that on long standing (or in vacuum) these crystals lose their solvent of crystallization (both methanol and water) and become amorphous.

4.3. Physical measurements

Microanalyses (C, H, N) were performed in a Perkin-Elmer 240C elemental analyzer. Mass spectra were recorded on a Perkin Elmer (USA) Flexer SQ 300 MS Mass Spectrometer operating in ESI mode. Infrared and far-infrared spectra were measured with a Jasco IR report-100 and a Shimadzu IR Affinity - 1 FT-IR spectrometer using KBr pellet. Electronic absorption spectra were recorded on a Jasco V-570 UV/VIS/NIR spectrophotometer using a pair of matched quartz cell of path length of 1 cm. Electron paramagnetic resonance spectra were recorded on a JEOL, Japan Model: JES - FA200 ESR spectrometer with X and Q band. Room temperature solution EPR spectra were recorded using an aqueous cell and frozen glass spectra were recorded in liquid nitrogen using a quartz dewer. Conductivity measurement was done using a Mettler Toledo dual conductivity/pH meter model SevenMulti equipped with Inlab 730 and Inlab 413 electrodes. Electrochemical measurements were done with the help of a Bioanalytical system CV-27 electrochemical analyzer and a BAS model X-Y recorder at 298K under dinitrogen. A standard three electrode cell consisting of a platinum working electrode, a platinum auxiliary electrode and a Ag/AgCl reference electrode was used. Tetrabutylammonium perchlorate ($[N(n\text{-}Bu)_4]ClO_4$) was used as supporting electrolyte.

4.4. X-ray crystallography

4.4.1. 1,5-Bis(salicylidene)carbohydrazide, (o-$HOC_6H_4CH=NNH)_2C=O$

Colourless crystals were obtained from the slow evaporation of a methanolic-ethanol (1:1) solution of 1,5-Bis(salicylidene)carbohydrazide (LIGAND) at room temperature. A crystal with approximate size of $0.3 \times 0.2 \times 0.2$ mm was mounted on a Bruker Axs Kappa Apex2 diffractometer equipped with graphite-monochromated [Mo Kα, $\lambda = 0.71073$ Å] radiation. The unit cell parameters (Table 3) were determined by the method of difference vectors using reflections scanned from three different zones of the reciprocal lattice. The intensity data were measured using ω and φ scan with frame width of 0.5°. The frames integration and data reduction were performed using Bruker SAINT-Plus (Version 7.06a) software [33]. The multi-scan absorption corrections were applied to the data using SADABS software. The crystal is indexed in Orthorhombic system with space group Aba2 and lattice parameters $a = 14.5381(18)$ Å, $b = 9.3483(11)$ Å, $c = 10.2927(11)$ Å, $\alpha = 90^{o}$, $\beta = 90^{o}$, $\gamma = 90^{o}$. SIR-92 program [34] was used for solving the structure. Structure was refined using SHELXL-2014 (Sheldrick, 2014) program [35]. Successive difference fourier map showed the positions of all hydrogen atoms. However, the hydrogen positions were geometrically fixed and refined through riding model. The full matrix structure refinement was carried out through minimization of the function $\sum(w(F^2_o - F^2_c))^2$, where $w = [\sigma^2 (F^2_o) + (0.\ 0.0389P)^2 + 0.6887P]^{-1}$ and $P = (F^2_o + 2F^2_c)/3$, F^2_o is the measured intensity (i.e., intensity observed) and F^2_c is the intensity calculated. The final residual factors were $R = 0.03$ and $wR = 0.0893$. The largest difference map peak was 0.139 e/Å^3.

4.4.2. [Zn(o-phen)LCu(OAc)]0.5H_2O·0.5CH_3OH (COMPLEX **3**)

Blue crystals were obtained from the slow evaporation of a methanolic solution of compound **3** at room temperature. A crystal with approximate size of $0.3 \times 0.2 \times 0.2$ mm was mounted on a Bruker Axs Kappa Apex2 diffractometer equipped with graphite-monochromated [Mo Kα, $\lambda = 0.71073$ Å] radiation. The unit cell parameters (Table 3) were determined by the method of difference vectors using reflections scanned from three different zones of the reciprocal lattice. The intensity data were measured using ω and φ scan with frame width of 0.5°. The frames integration and data reduction

were performed using Bruker SAINT-Plus (Version 7.06a) software [33]. The multi-scan absorption corrections were applied to the data using SADABS software. The crystal is indexed in triclinic system with space group P$\bar{1}$ and lattice parameters a = 12.473(2) Å, b = 15.955(3) Å, c = 16.000(3) Å, α = 77.052(11)°, β = 67.897(9)° , γ = 89.979(10)°. SIR-92 program [34] was used for solving the structure. Structure was refined using SHELXL-2014 (Sheldrick, 2014) program [35]. Successive difference fourier map showed the positions of all hydrogen atoms. However, the hydrogen positions were geometrically fixed and refined through riding model. The full matrix structure refinement was carried out through minimization of the function$\sum(w(F^2_o - F^2_c))^2$, where $w = [\sigma^2 (F^2_o) + (0.1626P)^2 + 116.3643P]^{-1}$ and $P = (F^2_o + 2F^2_c)/3$, F^2_o is the measured intensity (i.e., intensity observed) and F^2_c is the intensity calculated. The final residual factors were R = 0.11 and wR = 0.3351. The largest difference map peak was 0.853 e/Å^3.

Table 3. Crystal data and structure refinement for LIGAND and COMPLEX **3**.

Identification code	LIGAND	COMPLEX **3**
Empirical formula	$C_{15}H_{14}N_4O_3$	$C_{29.50}H_{24}CuN_6O_6Zn$
Formula weight	298.30	687.46
Temperature	293(2) K	293(2) K
Wavelength	0.71073 Å	0.71073 A
Crystal system	Orthorhombic	Triclinic
Space group	A b a 2	P$\bar{1}$
Unit cell dimensions	a = 14.5381(18) Å	a = 12.473(2) Å
	b = 9.3483(11) Å	b = 15.955(3) Å
	c = 10.2927(11) Å	c = 16.000(3) Å
	α = 90°	α = 77.052(11)°
	β = 90°	β = 67.897(9)°
	γ = 90°	γ = 89.979(10)°
Volume	1398.8(3) Å^3	2862.8(9) Å^3
Z	4	4
Density (calculated)	1.416 Mg/m^3	1.595 Mg/m^3
Absorption coefficient	0.102 mm^{-1}	1.636 mm^{-1}
F(000)	624	1400

Crystal size	0.300 x 0.200 x 0.200 mm^3	0.300 x 0.200 x 0.200 mm^3
Theta range for data collection	2.802 to 24.996°.	1.315 to 17.653°
Index ranges	-17<=h<=17, -11<=k<=10, -12<=l<=12	-10<=h<=10, -13<=k<=13, -13<=l<=13
Reflections collected	8223	17755
Independent reflections	1228 [R(int) = 0.0308]	3296 [R(int) = 0.1213]
Completeness to theta	= 25.000° 99.7 %	= 25.242° 31.8 %
Absorption correction	Semi-empirical from equivalents	Semi-empirical from equivalents
Max. and min. transmission	0.971 and 0.942	0.762 and 0.601
Refinement method	Full-matrix least-squares on F^2	Full-matrix least-squares on F^2
Data / restraints / parameters	1228 / 1 / 109	3296 / 573 / 821
Goodness-of-fit on F^2	1.115	1.094
Final R indices [I>2sigma(I)]	R1 = 0.0339, wR2 = 0.0795	R1 = 0.1062, wR2 = 0.2724
R indices (all data)	R1 = 0.0448, wR2 = 0.0893	R1 = 0.1755, wR2 = 0.3351
Extinction coefficient	n/a	0.0059(12)
Largest diff. peak and hole	0.139 and -0.141 e.$Å^{-3}$	0.853 and -0.797 e.$Å^{-3}$

4.5. Methods for biological activity

4.5.1. DNA binding studies

Electronic spectra of the compounds **1-3** with incremental amounts of calf thymus DNA (ct-DNA) have been recorded using a Jasco V-570 UV/VIS/NIR spectrophotometer in order to get the binding constant for the compounds. The absorption titration experiments were performed by keeping the complex concentration constant and by varying the concentration of ct-DNA from 0 to 40 μM in 10 mM Tris–HCl buffer (pH 7.43).

4.5.2. Cytotoxicity studies

4.5.2.1. Cell culture and treatment

The human cancer cell lines A549, MCF7 and normal human keratinocyte HaCaT cells and human lung embryonic L132 cells were purchased from NCCS Pune. All the cell lines were cultured in T-25 mm NUNC Cell culture flasks with DMEM High glucose medium with 10% Fetal Bovine Serum

(GIBCO performance plus grade, US origin) supplemented with penicillin (100 units/ml), streptomycin (100 µg/ml) Gentamycin 50µg/mL and amphotericin B (2.5 µg/ml) at 37°C (5% CO_2 and 95 % $O_{2)}$ in a CO_2 incubator. The cells were sub cultured after they had reached 70-80 % confluence by trypsinization and used for further experimental purpose.

4.5.2.2. 3-(4,5-Dimethylthiazol-2-yl)-2,5-diphenyltetrazolium bromide (MTT) assay

MTT assay was performed to evaluate the cytotoxicity of the compounds on cancer and normal cell lines. In this assay, cell viability was determined by the reduction of yellow MTT into purple formazan product by the enzymatic activity of mitochondrial dehydrogenase in the live cells based on the method of Mabley et al. [36]. The cells were plated on 96 well plates at a density of 4×10^4 per well and treated with complexes **1**, **2**, and **3** as described at varying concentration starting from 0.25µM, 0.5µM, 0.75µM, 1 µM, 2.5µM, 5µM and 10µM was added with DMEM culture medium containing 10%FCS. The MTT assay was carried out in triplicates. After 24 hour incubation, the cells were examined under phase contrast microscope and observed the cells morphology and photographed using Leica systems. Subsequently, the medium was removed and the cells were treated with 0.5mg/ml of MTT (Thiazolyl Blue Tetrazolium Bromide salt) in 1X PBS (150µL/well) and incubated for 4 hours in a CO_2 incubator. Following 4 incubation with MTT solution, the solution was removed and blue colored formazan crystal was solubilized with 200 µL DMSO. The absorbance was measured at 570 nm using BioRad ELISA plate reader.

4.5.2.3. Cellular morphology assessment. Acridine orange (AO)/ Propidium iodide (PI) dual staining

A549 cells and HaCaT cells were plated in 6-well plates at a density of 5×10^4, and were allowed to grow at 37°C in a humidified CO_2 incubator until they were 70–80% confluent. The cells were then treated with different concentrations of complexes **1**-**3** (0.5, 1, and 2 µM) for 24 h. The culture medium was aspirated from each well and cells were gently rinsed twice with PBS at room temperature. Equal volumes of cells from control and metal complex treated were stained with 1

µg/mL of acridine orange and propidium iodide and incubated in the dark for 30 min, then viewed with Leica fluorescence microscope.

Acknowledgements

We thank the SAIF, IIT-Madras for XRD facilities; and SAIF, IIT-Bombay for recording EPR of the compounds **1-3** using JEOL, Japan Model: JES - FA200 ESR spectrometer. A.P.K. thanks Mr. Atanu Banerjee and Dr. Rupam Dinda, Department of Chemistry, National Institute of Technology, Rourkela, India for help with the ESI-MS results. A.P.K. thanks Mr. Srimanta Haldar and Dr. P. Bhavana, Department of Chemistry, BITS-Pilani K. K. Birla Goa Campus for help with the electrochemical studies. P.T.M. thanks the SERB/DST, Govt. of India for a research Scheme EMR/2016/000745 and the INSA for the scheme SP/IHS/2016.

Appendix A. Supplementary material

Fig. S1. ESI-MS of the compounds **1-3.** Fig. S2. IR spectra of compounds **2** and **3** in KBr. Fig. S3. Electronic spectra of the compounds. Fig. S4. Electronic spectral change for the reaction of the compounds **1**-**2** with 3,5-DTBC. Fig. S5. Packing of the 1,5-Bis(salicylidene)carbohydrazide molecules in the unit cell. Fig. S6. Packing of Zn(o-phen)LCu(OAc)·0.5H_2O·0.5CH_3OH in the unit cell. Tables S1-S6. Crystal data and structure refinement for LIGAND, complex 3 and their bond lengths and bond angles. Crystallographic data for the structural analysis have been deposited with the Cambridge Crystallographic Data Center, numbers are CCDC 1546215 for the ligand and CCDC 1546227 for complex **3**, respectively. These data can be obtained free of charge via http://www.ccdc.cam.ac.uk/conts/retrieving.html, or from the Cambridge Crystallographic Data Centre, 12 Union Road, Cambridge CB2 1EZ, UK; Fax: (+044) 1223-336-033; or E-mail: deposit@ccdc.cam.ac.uk.

References

[1] (a) R.C. Todd, S.J. Lippard, Metallomics, 1 (2009) 280–291; (b) C.X. Zhang, S.J. Lippard, Currn. Opin. Chem. Biol. 7 (2003) 481-489; (c) P. Nagababu, A.K. Barui, B. Thulasiram, C. Shobha Devi, S. Satyanarayana, C.R. Patra, B. Sreedhar, J. Med. Chem. 58 (2015) 5226−5241; (d) C. Santini, M. Pellei, V. Gandin, M. Porchia, F. Tisato, C. Marzano, Chem. Rev. 114 (2014) 815−862.

[2] (a) M. Chauhan, K. Banerjee, F. Arjmand, Inorg. Chem. 46 (2007) 3072−3082; (b) S. Ramakrishnan, S., M. Palaniandavar, J. Chem. Sci. 117 (2005) 179−186; (c) J. Lu, Q. Sun, J.-L. Li, L. Jiang,W. Gu, X. Liu, Jin-Lei Tian, Shi-Ping Yan, J. Inorg. Biochem. 137 (2014) 46–56.

[3] S.K. Mal, M. Mitra, G. Kaur, V.M. Manikandamathavan, M.S. Kiran, A. Roy Choudhury, B. Unni Nair, R. Ghosh, RSC Adv., 4 (2014) 61337–61342.

[4] (a) U. Basu, I. Khan, A. Hussain, P. Kondaiah, A. R. Chakravarty, Angew. Chem., Int. Ed., 51 (2012) 2658-2661; (b) U. Basu, I. Khan, D. Koley, S. Saha, P. Kondaiah, A. R. Chakravarty, J. Inorg. Biochem., 116 (2012) 77 – 87; (c) R. Vijayalakhmi, M. Kanthimathi, R. Parthasarathi, B. U. Nair, Bioorg. Med. Chem., 14 (2006) 3300-3306.

[5] (a) M. G. Walker, V. Gonzalez, E. Chekmeneva, J. A. Thomas, Angew. Chem., Int. Ed., 51 (2012) 12107- 12110; (b) C. Fabbro, H. Ali-Boucetta, T. D. Ros, K. Kostarelos, A. Bianco and M. Prato, Chem. Commun., 48 (2012) 3911- 3926; (c) N. J. Farrer, L. Salassa and P. J. Sadler, Dalton Trans., (2009) 10690- 10701.

[6] (a) S. Rajalakshmi, M. S. Kiran, B. U. Nair, Eur. J. Med. Chem., 80 (2014) 393-406.
(b) S. Rajalakshmi, T. Weyherm¨uller, M. Dinesh, B. U. Nair, J. Inorg. Biochem., 117 (2012) 48-59.

[7] (a) T. K. Goswami, S. Gadadhar, M. Roy, M. Nethaji, A. A. Karande, A. R. Chakravarty, Organometallics, 31 (2012) 3010-3021; (b) T. K. Goswami, B. V. S. K. Chakravarthi, M. Roy, A. A. Karande, A. R. Chakravarty, Inorg. Chem., 50 (2011) 8452-8464.

[8] (a) M. Devereux, D. O. Shea, A. Kellett, M. McCann, M. Walsh, D. Egan, C. Deegan, K. Kedziora, G. Rosair, H. Muller-Bunz, J. Inorg. Biochem., 101 (2007) 881-892; (b) M. O'Connor, A. Kellett, M. McCann, G. Rosair, M. McNamara, O. Howe, B. S. Creaven, S. McClean, A. Foltyn-Arfa Kia, D. O'Shea, M. Devereux, J. Med. Chem., 55 (2012) 1957-1968.

[9] S. Tardio, I. Basanetti, C. Bignardi, L. Elviri, M. Tegoni, C. Mucchino, O. Bussolati, R. Franchi-Gazzola, L. Marchio, J. Am. Chem. Soc., 133 (2011) 6235-6242.

[10] (a) V. Rajendiran, R. Karthik, M. Palaniandavar, H. Stoeckli-Evans, V.S. Periasamy, M. A. Akbarsha, B.S. Srinag, H. Krishnamurthy, Inorg. Chem. 46 (2007) 8208-8221; (b) S. Ramakrishnan, V. Rajendiran, M. Palaniandavar, V.S. Periasamy, B.S. Srinag, H. Krishnamurthy, M.A. Akbarsha, Inorg. Chem., 48 (2009) 1309-1322.

[11] D. Dey, G. Kaur, A. Ranjani, L. Gayathri, P. Chakraborty, J. Adhikary, J. Pasan, D. Dhanasekaran, A.R. Choudhury, M. A. Akbarsha, N. Kole, B. Biswas, Eur. J. Inorg. Chem. (2014) 3350-3358.

[12] P. Adak, B. Ghosh, A. Bauza, A. Frontera, A. J. Blake, C. M. Corbella, C. Das-Mukhopadhyay, S. K. Chattopadhyay, RSC Adv. 6 (2016) 86851-86861.

[13] R.A. Festa, D.J. Thiele, Curr. Biol. 21 (2011) 877-883.

[14] G. Barone, A. Terenzi, A. Lauria, A. M. Almerico,J.M. Leal, N. Busto, B. García, Coord. Chem. Rev. 257 (2013) 2848-2862, and references therein.

[15] (a) A. Draksharapu, A.J. Boersma, M. Leising, A. Meetsma, W.R. Browne, Gerard Roelfes, Dalton Trans. 44 (2015) 3647-3655; (b) V.M. Manikandamathavan, T. Weyhermüller, R. P. Parameswari, M. Sathishkumar, V. Subramanian, B.U. Nair, Dalton Trans., 43 (2014) 13018–13031; (c) D.J. Arndt Jovin and T.M. Jovin, Methods Cell Biol., 30 (1989) 417-448.

[16] J.G. Da Silva, A.A. Recio Despaigne, S.R.W. Louro, C.C. Bandeira, E.M. Souza-Fagundes, H. Beraldo, European J. of Med. Chem. 65 (2013) 415-426.

[17] A.D. Tiwari, A.K. Mishra, S.B. Mishra, B.B. Mamba, B. Maji, S. Bhattacharya, Spectrochim. Acta Part A 79 (2011) 1050-1056.

[18] C. Marzano, M. Pellei, F. Tisato, C. Santini, Anti-Cancer Agents in Med. Chem. 9 (2009) 185-211, and references therein.

[19] Cheng-Yong Zhou, J. Zhao, Yan-Bo Wu, Cai-Xia Yin, P. Yang, J. Inorg. Biochem. 101 (2007) 10-18.

[20] J. Liu, T. Zhang, T. Lu, L. Qu, H. Zhou, Q. Zhang, L. Ji, J. Inorg. Biochem. 91 (2002) 269-276.

[21] F. Tisato, C. Marzano, M. Porchia, M. Pellei and C. Santini, Med. Res. Rev. 30 (2010) 708-749.

[22] V.M. Manikandamathavan, B.U. Nair, Eur. J. Med. Chem. 68 (2013) 244-252.

[23] B.M. Zeglis, V.C. Pierre, J.K. Barton, Chem. Commun. 44 (2007) 4565-4579.

[24] S.S. Bhat, A.A. Kumbhar, H. Heptullah, A.A. Khan, V.V. Gobre, S.P. Gejji, V.G. Puranik, Inorg. Chem. 50 (2011) 545-558.

[25] K.M. Guckian, B.A. Schweitzer, R.X. Ren, C.J. Sheils, D.C. Tahmassebi, E.T. Kool, J. Am. Chem. Soc. 122 (2000) 2213-2222.

[26] K.M. Guckian, T.R. Krugh, E.T. Kool, J. Am. Chem. Soc. 122 (2000) 6841-6847.

[27] (a) D.D. Li, J.L. Tian, W. Gu, X. Liu, H.H. Zeng, S.P. Yan, J. Inorg. Biochem. 105 (2011) 894-901; (b) V.M. Manikandamathavan, V. Rajapandian, A.J. Freddy, T. Weyhermuller, V. Subramanian, B.U. Nair, Eur. J. Med. Chem. 57 (2012) 449-458.

[28] M.K. Koley, Om P.Chouhan, S. Biswas, J. Fernandes, A. Banerjee, A. Chattopadhyay, B. Varghese, P.T. Manoharan, A.P. Koley, Inorg. Chim. Acta 456 (2017) 179–198.

[29] (a) C. Bustos, O. Burckhardt, R. Schrebler, D. Carrillo, A.M. Arif, A. H. Cowley, C.M. Nunn, Inorg. Chem. 29 (1990) 3996-4001; (b) D. Dragancea, A.W. Addison, M. Zeller, L.K. Thompson, D. Hoole, M.D. Revenco, A.D. Hunter, Eur. J. Inorg. Chem. (2008) 2530-2536.

[30] L.J. Frrugia. J. Appl. Cryst., 30 (1997) 565-566.

[31] F. Gao, H. Chao, F. Zhou, Y.-X. Yuan, B. Peng, L.-N. Ji, J. Inorg. Biochem. 100 (2006) 1487-1494.

[32] W. D. Wilson, L. Ratmeyer, M. Zhao, L. Strekowski, D. Boykin, Biochemistry 32 (1993) 4098-4104.

[33] Bruker-Nonius (2004). APEX-II and SAINT-Plus (Version 7.06a), Bruker AXS Inc., Madison, Wisconsin, USA.

[34] A. Altormare, G. Gascarano, C. Giacovazzo, A. Guagliardi. J. Appl. Cryst.. 26 (1993) 343.

[35] (a) G.M. Sheldrick. (2012). SHELXL Version 2012. University of Göttingen, Germany; (b) G.M. Sheldrick. (2014). SHELXL Version 2014. University of Göttingen, Germany.

[36] J.G. Mabley, W.L. Suarez-Pinzon, G. Hasko, A.L. Salzman, A. Rabinovitch, E. Kun, C. Br. Szabo, J. Pharmacol. 133 (2001) 909-919.

Graphical abstract

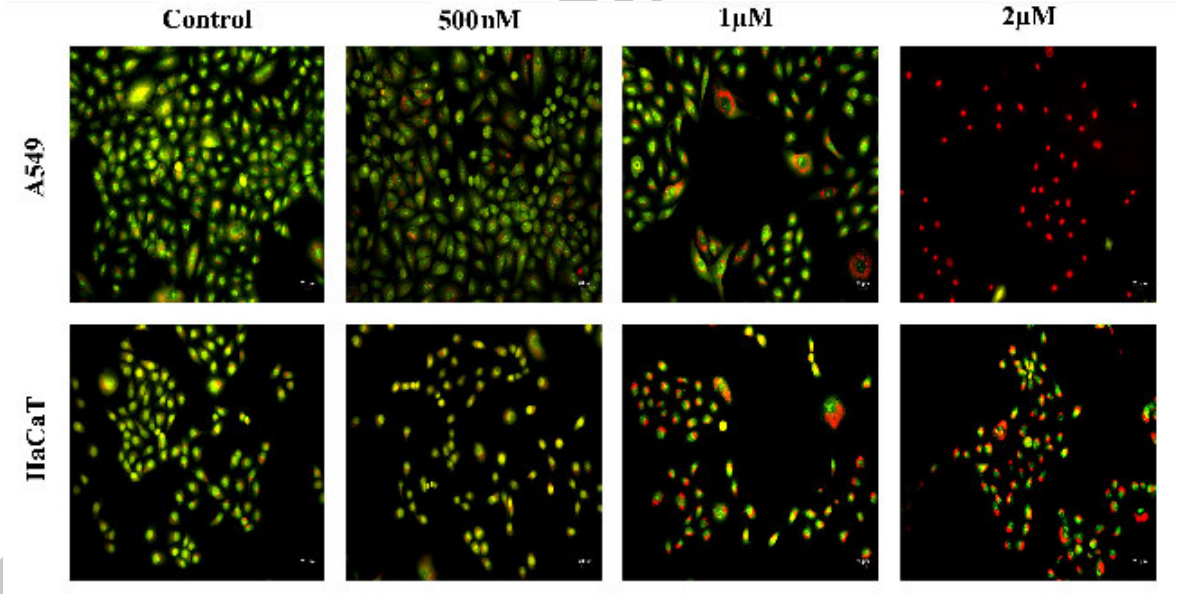

Cu(II)/Zn(II) complexes containing a carbohydrazone Schiff base ligand and 1,10-phenantroline as a coligand display remarkable cytotoxicity against the human lung cancer A549 cell line as well as the breast cancer MCF7 cell line as evident from the MTT assay. AO/PI dual staining assay for A549 and HaCaT cells suggest the apoptotic pathway for the anticancer activity of these complexes.

Highlights

- Copper(II) /zinc(II) complexes show intercalative DNA binding.
- Some of them possess catechol oxidation activity.
- Show remarkable cytotoxicity for the lung cancer A549 cell line.
- Also show significant cytotoxicity for the breast cancer MF7 cell line.
- In vitro AO/PI dual staining suggests an apoptotic pathway for their anticancer activity.

Figure Captions

Fig. 1. Structure of the ligand in its keto and enol forms.

Fig. 2. Proposed structures of the compounds **1-3**.

Fig. 3. Plot of absorbance change at ~401 nm for the formation of 3,5-DTBQ from the catalytic oxidation of 3,5-DTBC in presence of air with (1) 0.90×10^{-4} M **1** and 1.10×10^{-2} M 3,5-DTBC in DMSO (blue circles), (2) 0.72×10^{-4} M **2** and 1.10×10^{-2} M 3,5-DTBC in DMSO (black squares), (3) 0.75×10^{-4} M **2** and 1.10×10^{-2} M 3,5-DTBC in CH_3OH : DMSO (9:1) (red triangles).

Fig. 4. ORTEP diagram of the compound 1,5-bis(salicylidene)carbohydrazide.

Fig. 5. ORTEP diagram of the compound $Zn(o\text{-}phen)LCu(OAc)\cdot 0.5H_2O\cdot 0.5CH_3OH$.

Fig. 6. X-band EPR spectra of the compounds. (a)-(c) are RT spectra for **1**-**3** powder samples, (d)-(f) are LNT spectra for **1**-**3** powder samples, (g)-(i) are RT solution spectra for **1**-**3** in DMF, and (j)-(l) are LNT frozen glass spectra for **1**-**3** in DMF, respectively. * indicates the existence of the forbidden $\Delta Ms = \pm 2$ line around g~4.

Fig. 7. Change in electronic absorption spectra of **1**-**3** [5×10^{-5} M] upon titration with ct-DNA (0–40 μM) dissolved in 10 mM Tris–HCl buffer (pH 7.45). The arrow shows the decrease in absorbance

with respect to an increase in the concentration of ct-DNA. The figure in inset shows the linear fit of [DNA]/($\varepsilon_a - \varepsilon_f$) versus [DNA]. The binding constant (K_b) was calculated using the eqn. 1.

Fig. 8. MTT assay for the compounds **1**-**3**. Panel A. HaCaT cell line, panel B. L132 cell line, panel C. A549 cell line, and panel D. MCF7 cell line.

Fig. 9. Plot of cell viability versus concentrations of the compounds **1**, **2**, and **3**: panel A. HaCaT cell line, panel B. L132 cell line, panel C. A549 cell line, and panel D. MCF7 cell line.

Fig. 10. AO/PI staining results for compound **1** with A549 and HaCaT cell lines. Scale bar: 20 µm.

Fig. 11. AO/PI staining results for compound **2** with A549 and HaCaT cell lines. Scale bar: 20 µm.

Fig. 12. AO/PI staining results for compound **3** with A549 and HaCaT cell lines. Scale bar: 20 µm.

Fig. 13. Cyclic voltammogram of the compounds (1.5×10^{-3} mol L^{-1}) in DMF containing 0.1 M $[N(n\text{-}Bu)_4]ClO_4$ at a scan rate of 100 mV s^{-1}. Panel A for **1**, panel B for **2**, and panel C for **3**.